

Thermal properties of iron at high pressures and temperatures

Evgeny Wasserman and Lars Stixrude

Georgia Institute of Technology, Atlanta, Georgia 30332-0340

Ronald E. Cohen

Carnegie Institution of Washington, 5251 Broad Branch Road North West, Washington, DC 20015-1305

(Received 28 November 1995)

We investigate the thermoelastic properties of close-packed phases of iron at pressures up to 400 GPa and temperature to 6000 K using a tight-binding total-energy method and the cell model of the vibrational partition function. The calculated properties are in good agreement with available static and shock-wave experimental measurements. The compressional behavior of a number of thermoelastic parameters is found to resemble that of a prototypical oxide (MgO) supporting some aspects of universal behavior at high compression: the product of thermal expansivity α and bulk modulus is found to be nearly independent of compression at high pressure and the logarithmic volume derivative of α is found to decrease with compression. In contrast to the behavior of MgO, αK_T and δ_T of iron are found to depend strongly on temperature due to contributions from the thermal excitation of electrons. Significant decrease of the elastic constants of hcp iron with temperature was found.

I. INTRODUCTION

Understanding the properties of transition metals at high pressures and temperatures is a central problem of high pressure physics. Our relatively poor understanding of transition metals in these conditions contrasts with that of the simple oxides, where substantial progress has been made in recent years.¹⁻³ Experimental and theoretical investigation of simple oxides and silicates has revealed nearly universal behavior of a number of thermoelastic parameters at high temperatures and pressures. The product αK_T appears to be nearly independent of pressure and temperature for large compressions, and temperatures above the Debye temperature. Here we investigate whether similar universal behavior exists in transition metals. We apply an accurate tight-binding model to the investigation of the high pressure and temperature thermoelastic properties of iron and compare its properties with those of a simple oxide (MgO). We examine electronic and vibrational contributions to the thermal equation of state, and compare the thermoelastic behavior of Fe and MgO under high pressure and temperature conditions. The most important sources of experimental information on the thermal properties and subsolidus phase diagram of iron at high pressures and temperatures are shock-wave experiments,⁴ and static compression in the diamond anvil cell.⁵⁻⁷ The highest pressure and temperature data are from dynamic shock experiments. However, the measurements of temperature in shock experiments are extremely difficult for nontransparent materials like iron. The results of different groups (Refs. 4, 8, and 9) on the Hugoniot temperature at a given pressure differ by more than a thousand degrees. Theoretical calculations of thermal properties can help to resolve this issue but have so far been limited to simplified (e.g., pair potential) models of interatomic interactions, which contain substantial uncertainties.¹⁰

First-principles band structure calculations show that density functional theory in the generalized gradient approxima-

tion (GGA) yields a good description of the static equation of state and the low temperature phase diagram of iron.¹¹ The study of high temperature properties, however, is not feasible with the linearized augmented plane wave (LAPW) method used in this study. Simplified models of the electronic structure, in the form of low order moment approximations to the density of states, or effective potentials, are unlikely to be successful for predicting the high temperature properties of transition metals due to the complicated many-body nature of the interactions. For this reason, only a few molecular dynamics studies have addressed the thermodynamics of iron.^{10,12,13}

Here, we use a different approach to the study of transition metals at high pressures and temperatures. We combine an accurate tight-binding total-energy (TBTE) method with the cell model of the vibrational partition function. The TBTE method is grounded in accurate first-principles calculations—the parameters of the model are fitted to LAPW band structures and equations of state of nonmagnetic bcc, fcc, and hcp phases of iron over a wide range of volumes (40–90 bohr/atom). It has been previously shown that the TBTE model precisely reproduces LAPW results for Fe and accurately predicts equations of state, phase stabilities, elastic constants, and phonon dispersion curves of a number of transition metals.^{14,15} The TBTE model is nonorthogonal, and does not include pair potential or other structurally dependent non-band-structure terms. The parametrization is not performed in terms of coordination shells, since coordination shells are poorly defined in liquids and high temperature solids, rather the interactions decay smoothly with distance and vanish at 16.5 bohr. The tight-binding model is thousands of times more efficient computationally than LAPW calculations.

The cell model¹⁶⁻¹⁸ (also known as the particle in a cell method) is a mean field approximation to the thermal contribution to the Helmholtz free energy of crystalline phases. Each atom is confined to the Weigner-Seitz cell formed by its

nearest neighbors.¹⁶ Interatomic correlations and diffusion are ignored, so that the translational degrees of freedom of the atoms are separable. The partition function is then written in terms of a three-dimensional integral over the position of a single atom. Although interatomic correlations are neglected, the cell model includes anharmonic terms which are ignored in quasiharmonic lattice dynamics and which are likely important for temperatures which are a substantial fraction of the melting temperature. The cell model as applied here is a classical method for the vibrational degrees of freedom, and is applicable at temperatures above the Debye temperature where vibrational states are essentially fully populated, and below the melting temperature where collective motions and diffusion become important. The cell model has been demonstrated to match successfully the thermodynamic properties of the fcc Lennard-Jones crystal¹⁷ and sodium chloride¹⁸ calculated from Monte Carlo simulations. Moreover, the cell model permits very efficient computation of thermal properties as compared, for instance, with molecular dynamics simulations. This allows us to investigate a wide range of thermoelastic parameters, including high order derivatives of the free energy, over the entire range of pressures and temperatures relevant to the earth and to high pressure experiments.

II. TIGHT-BINDING TOTAL-ENERGY MODEL

The TBTE model used¹⁴ is based on a two-center, nonorthogonal Slater-Koster formulation. This TBTE model is different from previous models in that the total energy is given by the eigenvalue sum and there are no pair potentials or other structure-dependent terms. This avoids the ambiguity by choice of energy zeros for different band structures, as discussed by Cohen *et al.*¹⁴ The hopping Hamiltonian and overlap tight-binding interaction parameters between s , p , and d orbitals (like $ss\sigma$, $sp\sigma$, etc.) are assumed to have the form

$$P_i = (a_i + b_i) \exp[-c_i^2 r] f(r), \quad (1)$$

where r is the interatomic distance, and $f(r) = \{1 + \exp[(r - r_0)/\ell]\}^{-1}$ is a cutoff function with parameters $r_0 = 16.5$ bohr and $\ell = 0.5$ bohr. The P_i represent 20 parameters, ten each for the Hamiltonian and overlap matrices. The interactions are relatively long range, extending to more than three times the nearest-neighbor distance. This feature contrasts significantly with many conventional TB models which include only the nearest-neighbor interactions.¹⁹ The onsite terms D_{lk} of the Hamiltonian matrix (the index $l = s, p$, and d labels orbitals, and k labels atoms) are assumed to vary as a function of local ‘‘density’’ around each atom, ρ_k , defined as

$$\rho_k = \sum_j \exp(-d^2 r_{jk}) f(r_{jk}) \quad (2)$$

according to a finite strain polynomial

$$D_{lk} = e_l + g_l \rho_k^{2/3} + h_l \rho_k^{4/3} + i_l \rho_k^2. \quad (3)$$

Altogether, there are 73 fit parameters a_i , b_i , c_i , d , e_l , g_l , h_l , and i_l for a monoatomic substance. The parameters are determined by fitting to more than 4000 weighted input

data consisting of the total energy and band structures of nonmagnetic bcc, fcc, and hcp iron over a more than twofold range of volumes as well as a set of tetragonal strained structures between fcc and bcc at two volumes.¹⁴

The TBTE model used here is nonmagnetic. The reason for this is that the LAPW calculations demonstrate that local magnetic moments for fcc and hcp phases vanish for all non-negative pressures,^{20,21} and the magnetic effects are known to become unimportant at high pressure.

Since occupied and unoccupied states (up to 1 Ry above the static Fermi energy) were included in the fit, the method is appropriate to high temperature calculations where thermal excitations of electrons are important.¹⁴ The total energy at finite temperature T for the case of the TBTE model is given as the sum over the eigenvalues of the ideal lattice ϵ_i :

$$E_{\text{total}}(V, T) = E_{\text{band}}(V, T) = E_0(V) + E_{\text{el}}(V, T) = 2 \sum_i f_i \epsilon_i, \quad (4)$$

where

$$f_i = \{\exp[(\epsilon_i - \mu)/(k_B T)] + 1\}^{-1} \quad (5)$$

is the Fermi-Dirac occupation number, μ is the chemical potential, k_B is the Boltzmann constant, and the eigenvalues ϵ_i are assumed to be independent of temperature at constant lattice and nuclear positions. The sum is over all energy levels. The factor 2 is due to the spin degeneracy. The chemical potential μ is determined from the particle conservation equation

$$2 \sum_i f_i = N_{\text{el}}, \quad (6)$$

where $N_{\text{el}} = 8N$ is the total number of electrons in the system and N is the number of atoms.

III. CALCULATION OF THERMAL PROPERTIES

The Helmholtz free energy of the system can be written as

$$F(V, T) = E_0(V) + E_{\text{el}}(V, T) - TS_{\text{el}}(V, T) + F_{\text{vib}}(V, T), \quad (7)$$

where $E_0(V)$ is the zero-temperature energy, $E_{\text{el}}(V, T)$ is the contribution due to thermal electronic excitations, $S_{\text{el}}(V, T)$ is the electronic entropy, and $F_{\text{vib}}(V, T)$ is the phonon contribution to the free energy. To evaluate the first three terms on the right-hand side we assume that the existence of the lattice vibrations does not affect E_{el} and S_{el} and calculate these terms for the ideal lattice. The corresponding thermal properties of interest are then found from the appropriate thermodynamic expressions involving volume and temperature derivatives of $F(V, T)$. Whenever practical, these derivatives are evaluated analytically. The computational details of the electronic contribution to F are given in the next section. The phonon contribution to the free energy and other thermodynamic properties are treated with the cell model and are discussed in the succeeding section.

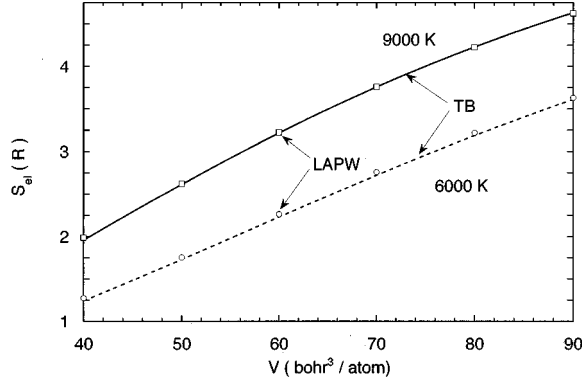


FIG. 1. Electronic entropy of hcp iron (in units of R) from self-consistent high temperature LAPW calculations (symbols) and from the TBTE method assuming temperature-independent eigenvalues (lines).

A. Electronic thermodynamics

The electronic entropy S_{el} is given by²²

$$S_{el} = -2k_B \sum_i f_i \ln f_i + (1 - f_i) \ln(1 - f_i). \quad (8)$$

This expression is valid for the entropy of a Fermi gas of (not necessarily free) particles.²³ $E_{band}(V, T)$ and $S_{el}(V, T)$ were calculated using primitive unit cells and the Monkhorst-Pack $16 \times 16 \times 16$ mesh of special k points for the Brillouin zone integration,²⁴ yielding 408 and 240 k points in the irreducible wedge of the Brillouin zone for fcc and hcp lattices, respectively. Tests showed that this mesh size is sufficient to reach convergence of the energy to within 0.1 mRy and of electronic entropy to within $0.003k_B/\text{atom}$.

The method for calculating the electronic entropy and energy is based on the assumption that the eigenvalues are temperature independent—only the occupation numbers depend on temperature, through the Fermi-Dirac distribution. We verify the validity of this approximation by comparing to self-consistent high temperature LAPW calculations. The Mermin theorem²⁵ generalizes the Hohenberg-Kohn density functional theory (DFT) to finite temperatures: the expression for the charge density is modified to include occupation numbers according to the Fermi-Dirac distribution. Possible explicit temperature dependence of the exchange-correlation energy is ignored. Following McMahan and Ross,²² we estimated the difference in the electronic contribution to thermodynamic properties calculated self-consistently from LAPW calculations at high temperature and those based on static eigenvalues. The self-consistent LAPW calculations with the GGA approximation for the exchange-correlation functional²⁶ were performed on hcp iron for volumes ranging from 40 to 90 bohr³/atom at temperatures $T=6000$ K and 9000 K. The Brillouin zone integration was carried out using the same $16 \times 16 \times 16$ mesh of special k points as for the TB calculation. The electronic entropy was then calculated from the eigenvalues and chemical potential according to Eq. (8). The comparison of calculated S_{el} is given in Fig. 1. As one can see from Fig. 1, the agreement between self-consistent LAPW calculations and TBTE calculations based on static eigenvalues is within 1%. We therefore confirm that this ap-

proximation is justified not only for iodine,²² but also for a transition metal. Therefore the TBTE model fitted to static band structures can be used to describe the electronic thermodynamics of the system with the required accuracy.

The electronic heat capacity $C_V^{el} = (\partial E_{band} / \partial T)_V$ is found by differentiating (4) with respect to temperature:

$$C_V^{el} = 2 \sum_i f_i (f_i - 1) \epsilon_i \left(-\frac{1}{k_B T} \frac{\partial \mu}{\partial T} - \frac{(\epsilon_i - \mu)}{k_B T^2} \right). \quad (9)$$

The temperature derivative of μ is determined by differentiating the conservation equation (6):

$$-\frac{1}{k_B T} \frac{\partial \mu}{\partial T} = \frac{1}{k_B T^2} \frac{\sum_i \Sigma f_i (f_i - 1) (\epsilon_i - \mu)}{\sum_i f_i (f_i - 1)}. \quad (10)$$

This is then substituted in Eq. (9).

The volume derivatives of the first three, nonvibrational, terms of the Helmholtz free energy (7) (denoted here as F_{NV}) were calculated using symmetric finite differences for $-\partial F / \partial V$ or alternatively by fitting the Birch-Murnaghan equation²⁷ to the $F_{NV}(V)$ isotherms and then differentiating the fit. Both methods agree within 0.3 GPa.

B. Vibrational contributions

Despite recent progress in the development of order- N methods for electronic structure calculations,¹⁹ TB molecular dynamics (TBMD) calculations of transition metals remain computationally very intensive. This stems from the fact that nine orbitals per atom have to be considered rather than four for s - p materials, and due to the long-range nature of the interactions in metals. In contrast, the computational burden of the cell model calculations is significantly less. At high temperatures the cell model becomes highly accurate. It includes on-site anharmonicity and neglects only defects, diffusion processes, and interatomic correlations. The cell model approximation yields a fairly accurate description of the equation of state of solid argon (represented with the Lennard-Jones model).¹⁷ It was also reasonably successful in describing the thermal expansivity and bulk modulus of an alkali halide crystal.¹⁸ Considering the computational limitations of TBMD for transition metals, we also believe that the cell model calculations may yield better estimates of the thermoelastic properties than averaging over necessarily short phase trajectories. Moreover, the Γ -point approximation to the Brillouin zone integrations, commonly used in TBMD, is questionable in a transition metal. Cell model calculations are a convenient tool to check the influence of this approximation and the effect of system size on the calculated thermal equation of state.

The cell model^{16,17} is an approximate way to evaluate the vibrational contribution F_{vib} to the Helmholtz free energy. The idea of the cell model is that the vibrational contribution to the partition function $Z_{cell} = \exp(-\beta F_{vib})$ where $\beta = (k_B T)^{-1}$, is calculated by having one “wanderer” particle move in the potential field of an otherwise ideal, static lattice.¹⁷

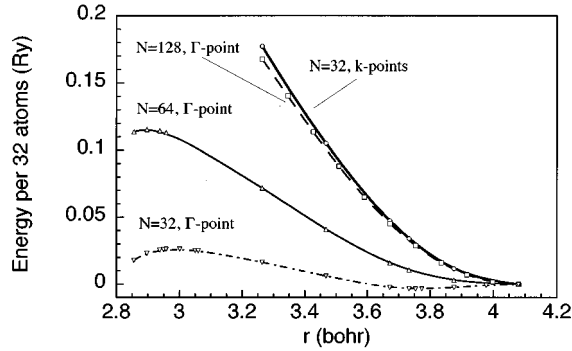


FIG. 2. Dependence of the perturbation energy for the fcc lattice when one atom is displaced towards its nearest neighbor. Note that the calculation with $N=128$ atoms and the Γ point (four supercells of 32 atoms stacked together) is adequate, while smaller supercells are not. The calculation with k -point sampling was done using a $4 \times 4 \times 4$ mesh of special k points.

$$Z_{\text{cell}} = \lambda^{-3N} \left[\int_{\Delta} \exp[-\beta(U(\mathbf{r}) - U_0)] d\mathbf{r} \right]^N, \quad (11)$$

where $\lambda = h/(2\pi mk_B T)^{1/2}$ is the de Broglie wavelength of the atoms, U_0 is the potential energy of the system with all atoms on ideal lattice sites, $U(\mathbf{r})$ is the potential energy of the system with the wanderer atom displaced by the radius vector \mathbf{r} from its equilibrium position, and N is the total number of atoms in the system. The integration is over the Wigner-Seitz cell Δ , centered on the equilibrium position of the wanderer atom. Since the cell model treats vibrations classically, it is expected to be a good approximation for temperatures greater than the Debye temperature of the solid but lower than the melting temperature.

We performed careful convergence tests of the perturbation energy with respect to the size of the supercell and the number of k points used in the Brillouin zone integrations. In a cubic 32-atom fcc supercell with periodic boundary conditions, we displaced one atom towards its nearest-neighbor and calculated the energy as a function of the nearest neighbor distance (Fig. 2). The perturbation energy is the energy difference between the distorted and the ideal lattice. The electronic temperature for this calculation was $T=4000$ K, and the volume $V=48$ bohr³/atom. We found that a $4 \times 4 \times 4$ k -point mesh (32 k points) was sufficient to accurately determine the energy of displacement in this supercell — denser meshes did not significantly alter the results. We investigate the effect of the size of the supercell by performing calculations in 32-, 64- and 128-atom supercells, using the Γ point only. The 64- and 128-atom supercells were formed by stacking two and four 32-atom cubic supercells together, respectively. In the 64- and 128-atom supercells two and four atoms were displaced, so that the geometrical configuration was the same in all cases. As one can see from Fig. 2, for small supercells ($N < 100$) the energy of displacement depends strongly on the size of the system when the Brillouin zone is sampled at a single point. Agreement between the 128-atom Γ point-only calculation and the 32-atom supercell with k points ($4 \times 4 \times 4$ mesh) calculation is excellent. Tests with even larger supercells (256 atoms) showed no significant change in the energy of displacement.

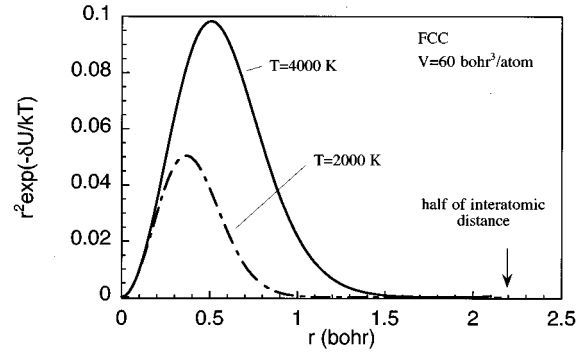


FIG. 3. Integrand in Eq. (11) along the first special direction (see text and Appendix) for the fcc phase ($V=60$ bohr³/atom) at temperatures $T=2000$ K and $T=4000$ K. Note the rapid decay of the integrand so that integration over the inscribed sphere is a good approximation to integration over the Wigner-Seitz cell.

We therefore used ~ 100 atom supercells for our cell model calculations. Our results also imply that molecular dynamics calculations of transition metals which use only the Γ -point require at least ~ 100 atoms in the unit cell.

The cell model calculations were performed on supercells of $N=108$ atoms for the fcc lattice and $N=128$ atoms for the hcp lattice with periodic boundary conditions. The distance between the “wanderer” atom and its nearest image was greater than the cutoff radius of the TB model. Integration over the Wigner-Seitz cell was replaced by integration over the inscribed sphere of radius equal to half the nearest-neighbor separation. We evaluate the effect of this spherical approximation by plotting the radial part of the integrand in Eq. (11), namely, $r^2 \exp[-\beta(U - U_0)]$, in Fig. 3 for two representative temperatures. As one can see from Fig. 3, the integrands decay rapidly and are essentially zero at the radius of the inscribed sphere. Similar decay of the integrands was found for the case of NaCl.¹⁸ The integration over the cell was therefore performed in spherical coordinates. The radial integration was performed using standard Gauss-Legendre quadrature. For the radial integration a 20-node quadrature was found to be sufficient for all properties, including the vibrational heat capacity C_V^{lat} , which we found to be most sensitive to the precision of integration.

To perform the integrations over the solid angle, we took advantage of the symmetry of the integrands. The integrands, being scalar functions, possess the point group symmetry of the lattice and the method of special directions²⁸ is appropriate. The numerical quadrature formulas are available for cubic lattices,²⁸ and we generalized this method for the hcp lattice (see the Appendix). The idea of this method is analogous to the Gauss-Legendre method in one dimension (1D). The integrand with the appropriate lattice symmetry is expanded in orthogonal lattice harmonics (cubic harmonics for the case of a cubic lattice). A quadrature formula (a set of directions and weights) for the solid angle integration $\int_0^{2\pi} d\phi \int_0^\pi \sin\theta f(\phi, \theta) d\theta$ is constructed in such a way that it exactly integrates as many lattice harmonics as possible for the given number of directions.

The convergence of the integration with respect to the number of special directions for the solid angle integration and the number of nodes for the radial integration is demonstrated in Tables I–III. Most of the calculations were per-

TABLE I. Convergence of the vibrational contribution to the Helmholtz free energy (F_{vib}) with respect to computational parameters.

Number of special directions	fcc phase, F_{vib} (mRy/atom)	
	$V=60 \text{ bohr}^3/\text{atom}$ $T=2000 \text{ K}, P=80 \text{ GPa}$	$V=70 \text{ bohr}^3/\text{atom}$ $T=3000 \text{ K}, P=45 \text{ GPa}$
1	-70.7	
2	-70.8	-152.8
4	-70.8	-152.8
Number of radial nodes	$V=60 \text{ bohr}^3/\text{atom}$	
	$T=2000 \text{ K}, P=80 \text{ GPa}$	$V=70 \text{ bohr}^3/\text{atom}$ $T=3000 \text{ K}, P=45 \text{ GPa}$
5	-71.7	
10	-70.8	-152.8
20	-70.8	-152.8
Number of special directions	hcp phase, F_{vib} (mRy/atom)	
	$V=60 \text{ bohr}^3/\text{atom}$ $T=2000 \text{ K}, P=76 \text{ GPa}$	$V=70 \text{ bohr}^3/\text{atom}$ $T=3000 \text{ K}, P=48 \text{ GPa}$
2	-182.1	
4	-182.1	-143.9
6	-182.0	-143.8

formed with a two-directional quadrature formula for the fcc lattice²⁸ (exact up to the cubic harmonic with $l_{\text{max}}=10$) and a four-directional quadrature formula for the hcp lattice (exact up to the lattice harmonic C_7^3). The computational efficiency of the special directions method is over an order of magnitude better than that of straightforward 3D integration; e.g., that of Cowley *et al.*,¹⁸ who used triple nine-point Gauss-Hermite quadrature with $9^3=729$ nodes.

The thermodynamic quantities of interest for the case of the cell model are calculated as derivatives of $F(V, T)$. Analytical derivatives were used in most cases. For the properties defined as temperature derivatives of F (e.g., lattice C_V) the expressions for the vibrational contribution have been given previously and are identical to those for systems interacting with pair potentials.¹⁷ The vibrational contribution to pressure P_{vib} is given by

$$P_{\text{vib}} = - \left(\frac{\partial F_{\text{vib}}}{\partial V} \right)_T = \frac{N}{\beta V} - \frac{N}{3V} \frac{\int_{\Delta} (\Xi - \Xi_0) \exp[-\beta(U - U_0)] d\mathbf{r}}{\int_{\Delta} \exp[-\beta(U - U_0)] d\mathbf{r}}, \quad (12)$$

TABLE II. Electronic entropy (in units of R) for the hcp phase calculated from self-consistent LAPW calculations at given temperature and from the TB fit to eigenvalues at $T=0 \text{ K}$ considering energy levels as independent of temperature.

V (bohr ³ /atom)	Self-consistent		TB	
	$T=6000 \text{ K}$	$T=9000 \text{ K}$	$T=6000 \text{ K}$	$T=9000 \text{ K}$
40	1.273	1.988	1.240	1.956
50	1.755	2.623	1.728	2.614
60	2.264	3.223	2.229	3.217
70	2.759	3.758	2.721	3.757
80	3.217	4.224	3.185	4.228
90	3.631	4.621	3.612	4.630

where Ξ is the virial of the system with the wanderer atom displaced by the radius vector \mathbf{r} from its equilibrium position, and Ξ_0 is the virial of the system with all atoms at their equilibrium positions. The virial is defined as the trace of the stress tensor.²⁹ This expression is obtained by differentiating $F_{\text{vib}} = -k_B T \ln Z$ with Z given by Eq. (11). The calculation of the virial is discussed in detail below. Consider a periodic system with unit-cell volume V_0 and atoms at positions \mathbf{R}_i , and also the scaled system with atoms at $a\mathbf{R}_i$ and volume $V = a^3 V_0$. Then the derivative of an arbitrary function of the atomic positions, $g(\mathbf{R})$, with respect to volume can be replaced by the derivative with respect to this scaling parameter :

$$\frac{\partial g(\mathbf{R})}{\partial V} = \lim_{a \rightarrow 1} \left(\frac{\partial g(\mathbf{R})}{\partial a} \frac{\partial a}{\partial V} \right) = \frac{1}{3V} \lim_{a \rightarrow 1} \left(a \frac{\partial g(\mathbf{R})}{\partial a} \right). \quad (13)$$

TABLE III. Convergence of the total pressure with respect to k -point sampling for fcc iron at $T=4000 \text{ K}$ ($N=108$ atoms in the cubic supercell). The vibrational contribution to pressure only was determined using the specified mesh size and the supercell. The thermal pressure for Γ -point ($\mathbf{k} = \mathbf{0}$) calculation was determined from the virial, while for the $2 \times 2 \times 2$ k -point mesh the virial was not calculated. The total pressure was therefore determined by fitting the finite strain polynomial to the calculated Helmholtz free energies as a function of volume along the isotherm and differentiating this polynomial with respect to volume. The error in pressure associated with this procedure is approximately 2 GPa.

V (bohr ³ /atom)	Static	P (GPa)	P (GPa)
	pressure (GPa)	(Γ -point)	($2 \times 2 \times 2$ mesh)
48	240	290	289
55	112	159	162
60	58	105	109
65	22	75	79
70	-2	62	65

We can therefore define the virial operator \hat{v} acting on $g(\mathbf{R})$ as

$$\hat{v}g = \lim_{a \rightarrow 1} \left(a \frac{\partial g(a\mathbf{R})}{\partial a} \right) \quad (14)$$

and the virial

$$\Xi = \hat{v}U = \lim_{a \rightarrow 1} \left(a \frac{\partial U(a\mathbf{R}_i)}{\partial a} \right), \quad (15)$$

where U is the potential energy of the system. It is well known³⁰ that for a system with periodic boundary conditions the virial *cannot* be calculated as $\Xi = -\sum_{i=1}^N \mathbf{F}_i \mathbf{R}_i$, \mathbf{F}_i being the force on the atom labeled i at the radius vector \mathbf{R}_i . For the case of a system interacting via pair potentials $V_{ij}(r_{ij})$ (15) yields the correct result:

$$\Xi = \frac{1}{2} \sum_{i,j} r_{ij} \frac{\partial V_{ij}}{\partial r_{ij}}.$$

For our TBTE method, the potential energy is given by E_{band} (4), and the virial is

$$\Xi = \sum_i \hat{v}(f_i \epsilon_i) = \sum_i f_i \hat{v} \epsilon_i + \epsilon_i \frac{\partial f}{\partial \epsilon_i} (\hat{v} \epsilon_i - \hat{v} \mu). \quad (16)$$

The result of the virial operator acting on the eigenvalues is evaluated by using the Hellmann-Feynman theorem

$$\frac{\partial \epsilon_i}{\partial a} = \frac{\langle \psi_i | \partial H / \partial a - \epsilon_i \partial S / \partial a | \psi_i \rangle}{\langle \psi_i | S | \psi_i \rangle}.$$

Here H and S are the Hamiltonian and overlap matrices, respectively, and $|\psi_i\rangle$ is the eigenvector corresponding to the eigenvalue ϵ_i . The derivatives of the matrix elements with respect to a are easily calculated because these are parametrized as analytical functions of the atomic coordinates \mathbf{R}_i , $i=1, \dots, N$, so that

$$\hat{v}A = \sum_i \mathbf{R}_i \frac{\partial A}{\partial \mathbf{R}_i}$$

where A is an element of the Hamiltonian or overlap matrix. Using the perturbation matrices $\hat{H} = \hat{v}H$ and $\hat{S} = \hat{v}S$ we obtain

$$\hat{v} \epsilon_i = \langle \psi_i | \hat{H} - \epsilon_i \hat{S} | \psi_i \rangle, \quad (17)$$

where we have used the fact that the eigenvectors are normalized such that $\langle \psi_i | S | \psi_i \rangle = 1$. For the case of a metal the Fermi level μ has a nonzero derivative with respect to the parameter a . It is determined by differentiating the conservation equation (6) with respect to this parameter:

$$\frac{\partial \mu}{\partial a} = \frac{\sum_i (\partial f / \partial \epsilon_i) (\partial \epsilon_i / \partial a)}{\sum_i (\partial f / \partial \epsilon_i)}. \quad (18)$$

The virial is then calculated by substituting Eq. (17) and Eq. (18) in Eq. (16), which yields

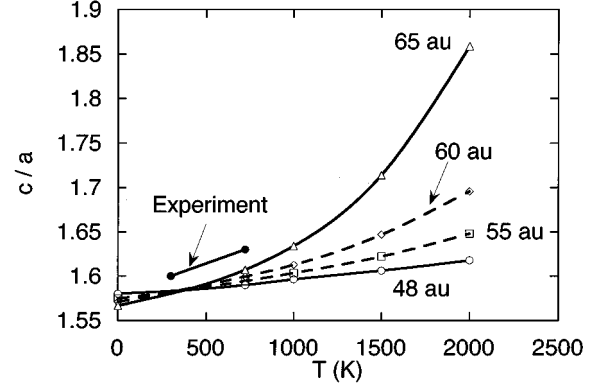


FIG. 4. Calculated and experimental (Ref. 45) temperature dependence of the c/a ratio for hcp iron.

$$\Xi = \sum_i \left[f_i \langle \psi_i | \hat{H} - \epsilon_i \hat{S} | \psi_i \rangle + \epsilon_i \frac{\partial f}{\partial \epsilon_i} \left(\langle \psi_i | \hat{H} - \epsilon_i \hat{S} | \psi_i \rangle - \frac{\sum_j (\partial f / \partial \epsilon_j) \langle \psi_j | \hat{H} - \epsilon_j \hat{S} | \psi_j \rangle}{\sum_j (\partial f / \partial \epsilon_j)} \right) \right] \quad (19)$$

The vibrational contribution to $\alpha K_T = (\partial P / \partial T)_V$ was obtained by differentiating (12) analytically with respect to temperature. The electronic contribution was evaluated by differentiating the appropriate terms of (1) analytically with respect to temperature and numerically with respect to volume.

IV. THERMAL PROPERTIES

Two close-packed phases of iron were considered, namely, fcc and hcp. For the hcp structure the equilibrium value c/a was determined from the condition that it yields the minimum of $F(c/a, V = \text{const}, T = \text{const})$. Plotted in Fig. 4 is the calculated temperature dependence of the c/a ratio for hcp iron at a set of volumes. The experimental result at a pressure of ~ 21 GPa corresponds approximately to $V = 65$ bohr³/atom. As one can see from Fig. 4, the calculations are consistent with the experimental result that the c/a ratio increases with temperature.

The volume-conserving strain associated with the change of c/a is described by the strain matrix $\vec{\epsilon} = \text{diag}\{e_1, e_1, (1 + e_1)^{-2} - 1\}$.³¹ The initial state is the hcp lattice with the equilibrium c/a ratio. The initial state is characterized by hydrostatic stress $\tau_i = -P$ for $i=1,2,3$ and $\tau_i = 0$ for $i=4,5,6$. The isothermal elastic constants C_{ij} are defined as expansion coefficients of the quadratic terms of a series expansion of F about the initial state.³²

$$\Delta F / V = \tau_i e_i + \frac{1}{2} C_{ij} e_i e_j. \quad (20)$$

Expanding e_3 in powers of e_1 ,

$$e_3 = (1 + e_1)^{-2} - 1 = -2e_1 + 3e_1^2 - 4e_1^3 + \dots, \quad (21)$$

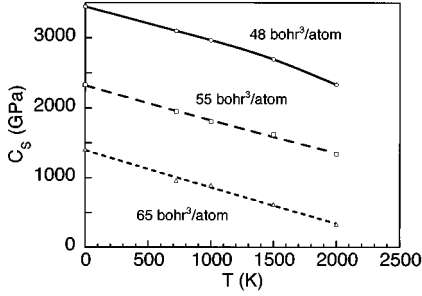


FIG. 5. Temperature dependence of the isothermal shear elastic constant C_S defined by Eq. (23) for volumes 48, 55, and 65 $\text{bohr}^3/\text{atom}$.

we obtain

$$\Delta F/V = e_1^2(C_{11} + C_{12} + 2C_{33} - 4C_{13}) + O(e_1^3). \quad (22)$$

Defining

$$C_S = C_{11} + C_{12} + 2C_{33} - 4C_{13}, \quad (23)$$

one obtains $\Delta F/V = C_S e_1^2 + O(e_1^3)$. The temperature dependence of the calculated isothermal shear elastic constant C_S is given in Fig. 5. As one can see from Fig. 4 and Fig. 5, the substantial increase of the c/a ratio with temperature is associated with a softening of the corresponding elastic constant C_S , and may be related to a high temperature mechanical instability.

The only source of information on the equation of state of iron at high compression and high temperatures is shock-wave data. The pressures P_H and temperatures T_H on the Hugoniot were calculated for a set of volumes ranging from 48 $\text{bohr}^3/\text{atom}$ to 65 $\text{bohr}^3/\text{atom}$ by solving the Rankin-Hugoniot equation:³³

$$\frac{1}{2} P_H(V_0 - V) = E_H - E_0. \quad (24)$$

For the zero-pressure energy E_0 and volume V_0 the LAPW results for the bcc phase were used.¹¹ The LAPW method correctly predicts the bcc-hcp phase transition at $P = 11$ GPa for $T = 0$ K. We considered the hcp phase for the Hugoniot calculation. For a given volume V , the temperature on the Hugoniot was varied until Eq. (24) is satisfied. The third-order Birch-Murnaghan equation²⁷ was then fitted to the calculated set of $P_H(V)$. Our approach does not invoke any empirical parameters and differs in this sense from that of Sherman and Jansen,³⁴ who used the Grüneisen parameter γ as an adjustable parameter to fit the experimental Hugoniot. We calculate the Hugoniot only for pressures greater than 13 GPa, the bcc-hcp transition pressure on the Hugoniot.

The agreement of the calculated Hugoniot with experimental data⁴ is good (Fig. 6). The discrepancy at pressures above 200 GPa can be attributed to phase transitions observed experimentally:⁴ a solid-solid phase transition to an unknown structure at $P = 200$ GPa and melting at $P = 243$ GPa. Figure 7 compares our calculated temperatures on the Hugoniot with previous model calculations⁴ and experimental measurements.^{8,9} Our result is approximately 1000 K lower than that of Yoo *et al.*⁸ but agrees well with the esti-

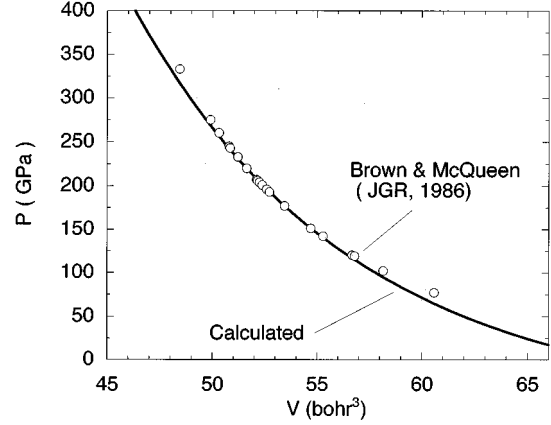


FIG. 6. Hugoniot for iron in the P - V plane. Solid line is the calculated Hugoniot for pressures above the bcc-hcp transition pressure. Circles are experimental measurements by Brown and McQueen (Ref. 4).

mates of Brown and McQueen.⁴ As mentioned above, experimental measurements of the Hugoniot temperatures disagree with each other. Excellent agreement between our calculations and the latest results of Gallagher and Ahrens⁹ suggests that Yoo *et al.*⁸ overestimate the Hugoniot temperature by approximately 1000 K.

The pressure at high temperatures can be written as

$$P(V, T) = P_0(V) + P_{\text{th}}(V, T), \quad (25)$$

where $P_0(V)$ is the static pressure and $P_{\text{th}}(V, T)$ is the thermal pressure. According to the Mie-Grüneisen equation, the thermal pressure is given as

$$P_{\text{th}}(V, T) = \frac{\gamma E_{\text{th}}(V, T)}{V}, \quad (26)$$

where E_{th} is the thermal contribution to the internal energy, and the *thermodynamic* Grüneisen parameter is defined by

$$\gamma \equiv V(\partial P / \partial E_{\text{th}})_V \equiv \frac{\alpha K_T V}{C_V}. \quad (27)$$

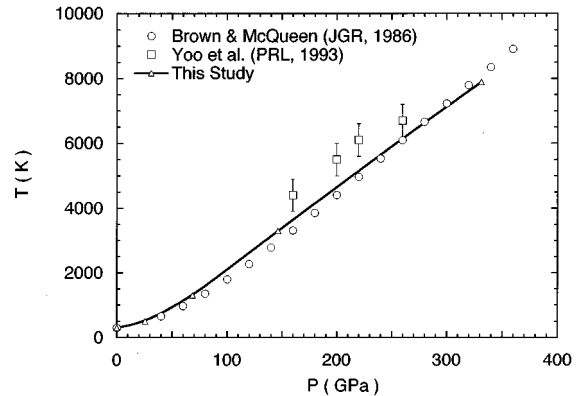


FIG. 7. Calculated temperature on the Hugoniot (solid line); squares are measurements by Yoo *et al.* (Ref. 8) and circles represent the thermodynamic calculations of Brown and McQueen (Ref. 4).

As one can see from the definition of the thermal expansivity $\alpha=(1/V)(\partial V/\partial T)_P$ and the bulk modulus $K_T=-V(\partial P/\partial V)_T$, the product αK_T is the temperature derivative of the thermal pressure. Therefore $P_{\text{th}}(V,T)=\int_0^T \alpha K_T dT$. The parameters defined above are widely used in high pressure research. The Grüneisen parameter $\gamma=V(\partial P/\partial E)_V$ along with total C_V (vibrational+electronic) is traditionally used to reduce shock compression data, for instance to transform between isotherms and Hugoniot.^{4,34} The temperature on the Hugoniot can be evaluated in the absence of phase transitions by integrating the thermodynamic equation

$$dT = -T \left(\frac{\gamma}{V} \right) dV + \frac{1}{2C_V} [(V_0 - V)dP + (P - P_0)dV] \quad (28)$$

along the Hugoniot.⁴

It is of interest to evaluate the validity and limitations of several assumptions often made in high P, T thermodynamic calculations: (1) independence of the parameter $\alpha K_T=(\partial P/\partial T)_V$ on temperature and compression, and (2) power law dependence of the Grüneisen parameter on compression, $\gamma=\gamma_0(V/V_0)^q$. The parameter αK_T , the product of two experimentally measurable quantities, is often used in high pressure calculations to transform from (P, T) to (V, T) space.³ Considering the lack of experimental data, it is desirable to find a parameter that remains approximately constant over a wide range of pressure and/or temperature. The αK_T parameter was argued³ to be such a universal temperature- and pressure-independent parameter for compressions $V/V_0 < 0.7$ and temperatures above the Debye temperature of the solid. We expect the cell model to provide an excellent test of these assumptions for iron—from the methodological point of view, the errors introduced by the cell model approximation in α and K_T are correlated¹⁸ in the sense that if one quantity is underestimated, the other one is overestimated. Therefore the product is expected to be estimated quite accurately. For the case of a metal, there are vibrational and electronic contributions. In order to highlight the contribution from the electrons in the conduction band, we compare the results for iron to those for a simple oxide, MgO, which contains no electronic contribution.

Plotted in Fig. 8 is the αK_T parameter for iron calculated in this study along with that for MgO taken from Ref. 1. The calculated αK_T [Figs. 8(a) and 8(b)] can be considered approximately independent of compression at high compressions but depends on temperature. For instance, at $V=60$ bohr³/atom, αK_T increases by approximately 40% from $T=1000$ K to $T=6000$ K. The temperature dependence αK_T is much stronger than and of the opposite sense to that found for MgO. As one can see from Fig. 8, the calculated vibrational contribution to αK_T decreases with temperature for both Fe and MgO due to anharmonic contributions (Ref. 32, p. 232). However, for iron this decrease is more than compensated by the electronic contribution. As one can see from Fig. 8(c), the electronic contribution to αK_T increases nearly linearly with temperature. This behavior at low temperatures has been observed in other metals at low temperature (Ref. 32, p. 288). For the free electron gas, αK_T also depends linearly on temperature.³⁵ Therefore the electronic

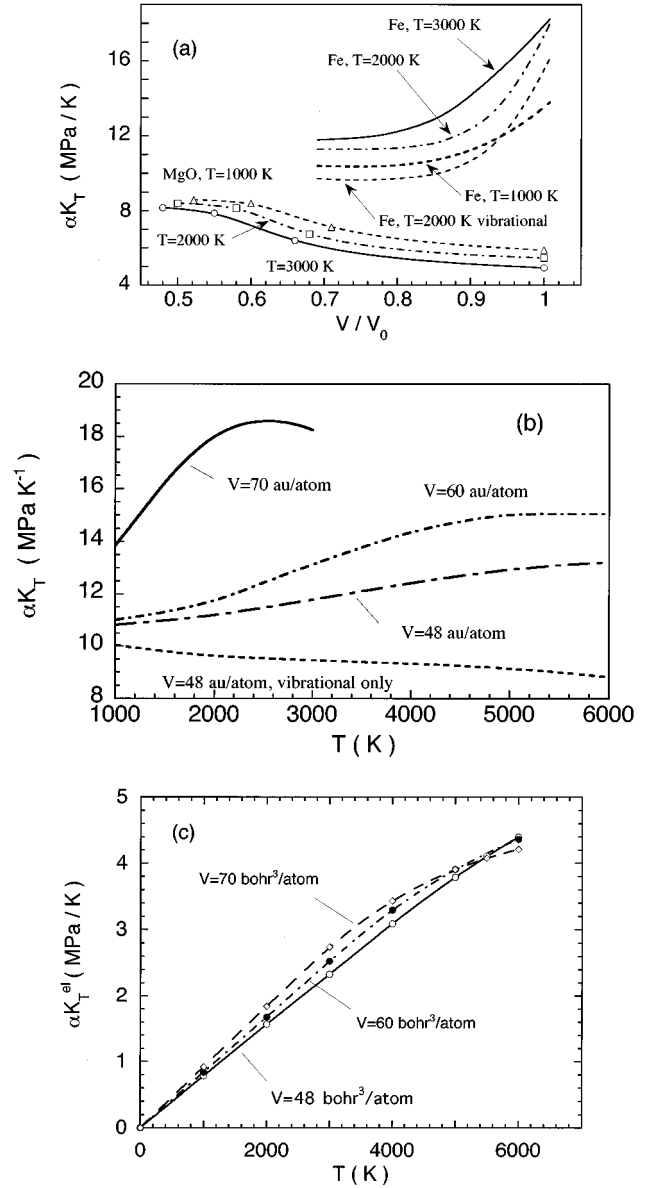


FIG. 8. Calculated temperature derivative of the pressure, αK_T , as a function of reduced volume (a) and as a function of temperature (b) of iron and MgO. The electronic contribution to αK_T in iron is plotted separately in (c). Note that the total αK_T is approximately independent of compression between $V=48$ and $V=60$ bohr³/atom, but its temperature dependence cannot be ignored even above the Debye temperature.

contribution is primarily responsible for the temperature dependence of αK_T for iron [Fig. 8(b)].

In our cell model calculations above the Debye temperature we found C_V^{lat} to increase with temperature. Nevertheless, we found that the Dulong-Petit value, $C_V^{\text{lat}}=3R$, is a reasonable approximation especially at high pressure, and may be suitable for the analysis of Hugoniot data. For instance, at $T=4000$ K $C_V^{\text{lat}}=3.12R$ and $3.18R$ at $V=48$ and 55 bohr³/atom, respectively.

The calculated electronic heat capacity (Fig. 9) for fcc iron has a linear temperature dependence at low temperatures. This result is expected from the Sommerfeld expansion, which yields:³⁵

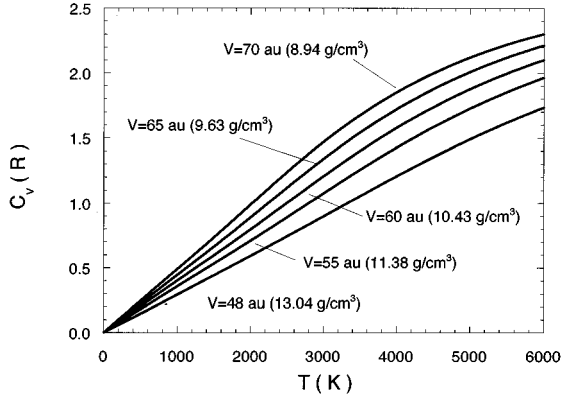


FIG. 9. Calculated electronic heat capacity of fcc iron. The curves correspond (from bottom to top) to increasing volumes $V=48, 55, 60, 65,$ and 70 bohr³/atom.

$$C_V^{\text{el}} = \Gamma T, \quad (29)$$

$$\Gamma = \frac{\pi^2}{3} k_B^2 V g(\epsilon_F) \quad (30)$$

where $g(\epsilon_F)$ is the density of states on the Fermi level at $T=0$ K. C_V^{el} at low temperatures can be written in a form similar to that for the free electron gas:

$$C_V^{\text{el}} = \left(\frac{\pi}{3}\right)^{2/3} m^* V n^{1/3} T, \quad (31)$$

where m^* is the effective electron mass for thermal properties, which accounts for the high density of states at the Fermi level in transition metals compared with the free electron gas, and n is the charge density.³⁵ The effective mass is proportional to the density of states at the Fermi level:

$$g(\epsilon_F) = 3^{1/3} \pi^{-4/3} m^* \hbar^{-2} n^{1/3}. \quad (32)$$

The calculated slope Γ of the linear portion of $C_V^{\text{el}} = \Gamma T$ at different volumes for the fcc phase is given in Table IV. It is compared to the free electron gas value, the ratio of these being the effective mass. The effective mass increases with volume, and at the zero-pressure density it approaches the experimentally observed value of $m^* \sim 8$.

The Sommerfeld expansion with two terms (30) ceases to be valid for iron at temperatures greater than around 4000 K. This is due to the existence of peaks in the density of states $g(\epsilon)$ near the Fermi level; therefore the higher order derivatives of $\epsilon g(\epsilon)$ are substantial. The temperature dependence

TABLE IV. Slope of the temperature dependence of the constant volume heat capacity for the fcc iron and the effective mass.

V (bohr ³ /atom)	From TB (mJ mol ⁻¹ K ⁻²)	For free electron gas (mJ mol ⁻¹ K ⁻²)	m^*/m_e
48	2.44	0.452	5.4
55	2.97	0.495	6.0
60	3.35	0.524	6.4
65	3.71	0.553	6.7
70	4.08	0.581	7.0

of the electronic heat capacity deviates from linearity, and tends to level off at high T . At high temperatures it is comparable to the lattice value $\sim 3R$. It has to be considered, therefore, when reducing shock-wave results. Our calculations of C_V^{el} agree with those of Bonnes and Brown,³⁶ who used the linear muffin tin orbital (LMTO) method in the atomic sphere approximation.

The Grüneisen parameter was calculated from its thermodynamic definition $\gamma = (\alpha K_T) V / C_V$. In the case of the cell model, it is easy to separate the vibrational or lattice contribution, γ_{lat} , and the electronic contribution, γ_{el} . The total Grüneisen parameter is then given by

$$\gamma = \frac{\gamma_{\text{el}} C_V^{\text{el}} + \gamma_{\text{lat}} C_V^{\text{lat}}}{C_V^{\text{el}} + C_V^{\text{lat}}}.$$

The lattice contribution is given separately in Fig. 10(a), and the total Grüneisen parameter in 10(b). Both calculated γ_{lat} and γ for iron increase significantly with volume. This increase is much more pronounced for iron than for MgO.¹ The temperature dependence of γ_{lat} is relatively weak. The lattice contribution dominates the total Grüneisen parameter at high compressions. The volume dependence of γ can be described approximately by a power law for compressions of interest for the shock-wave experiments. Plotted in Fig. 10(c) is the parameter $q \equiv (\partial \ln \gamma / \partial \ln V)_T$. As one can see from Fig. 10(c), it is not constant and a fit with constant q can be valid only over a limited region of volumes. Assuming a constant q gives only a moderate degree of accuracy; we found $q = 1.1$. A qualitatively similar volume dependence of q to that shown in Fig. 10(c) was found for model monatomic cubic lattices interacting via a variety of central-force potentials,³⁷ and in *ab initio* calculations of MgO.²

The calculated Grüneisen parameter was compared with experimental estimates by Jeanloz³⁸ and Brown and McQueen⁴ [Fig. 10(b)]. The results of Ref. 38 are based on the analysis of Hugoniot data for initially porous and nonporous samples and were fitted to the power law $\gamma = \gamma_0 (V/V_0)^q$. The agreement between our calculated Grüneisen parameter and the results of shock compression experiments is good.

There are three well-known approximate ways to calculate the Grüneisen parameter for a monoatomic solid, and we compare our cell model calculations to these approximate formulas. It is worth emphasizing, however, that the derivation of these expressions relies on assumptions that are not exactly satisfied in the case of our calculations. One can therefore expect only qualitative agreement with more accurate calculations. Even for a model fcc crystal interacting with pair potentials, no quantitative agreement was found between these approximate expressions and the results of a computer simulation.¹⁰ The three expressions can be combined in one using an integer parameter l to label the different expressions:³³

$$\gamma = -\frac{V}{2} \frac{\partial^2 (P V^{2l/3}) / \partial V^2}{\partial (P V^{2l/3}) / \partial V} + \frac{(l-2)}{3}. \quad (33)$$

The Slater approximation ($l=0$) considers the material as an elastic medium (Debye model) and ignores the volume dependence of Poisson's ratio. It yields $\gamma = K'/2 - 1/6$,

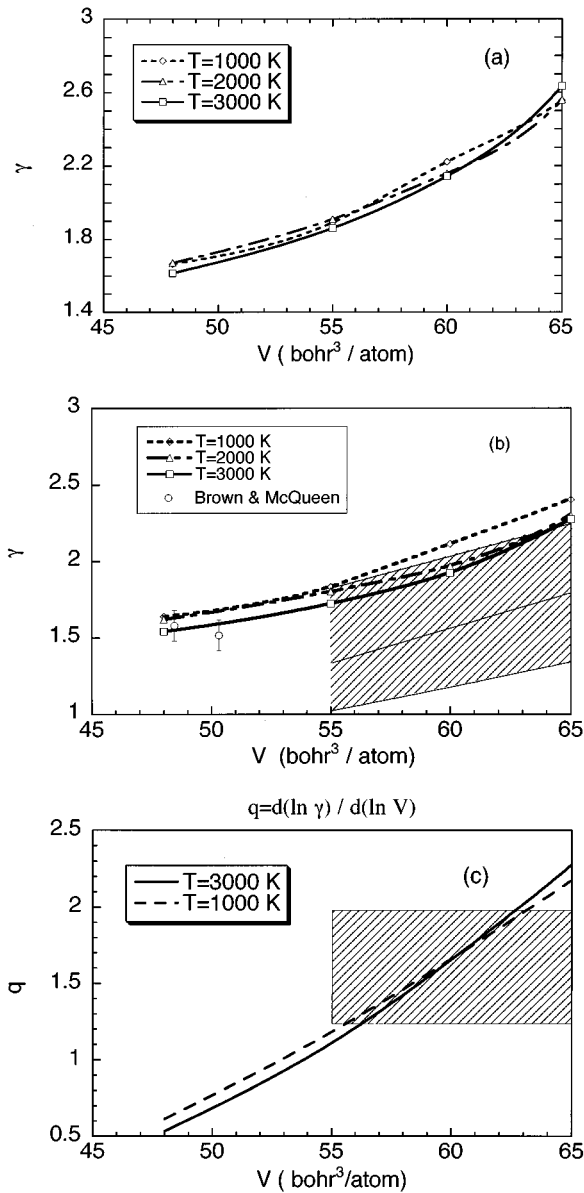


FIG. 10. Calculated lattice Grüneisen parameter γ_{lat} (a) and total Grüneisen parameter (b) compared to experimental measurements from Ref. 38 (thin solid line and a shaded confidence band) and Ref. 4 (circles). (c) Parameter q as a function of volume compared to Ref. 38 (solid line and shaded confidence band). Note that since γ increases with volume, the thermal pressure also increases with volume.

where $K' = (\partial K_T / \partial P)_T$ calculated at pressure P . The expression due to Dugdale and MacDonald ($l=1$) follows from the assumption that in a cubic crystal all the force constants have the same volume dependence. The expression for the free volume theory ($l=2$), in which the vibrations of atoms are considered in the spherically symmetric field of the neighbors, is exact for pairwise interactions between nearest neighbors only.³⁷ We evaluated γ for all the expressions using fourth-order Birch-Murnaghan fits to the static isotherms (Fig. 11). The expression by Slater ($l=0$) agrees best with our calculations. Still the discrepancy is substantial, especially at low compressions. Brown and McQueen⁴ assumed $\gamma V = \text{const}$. They estimated γ_0 to range from 1.7 to

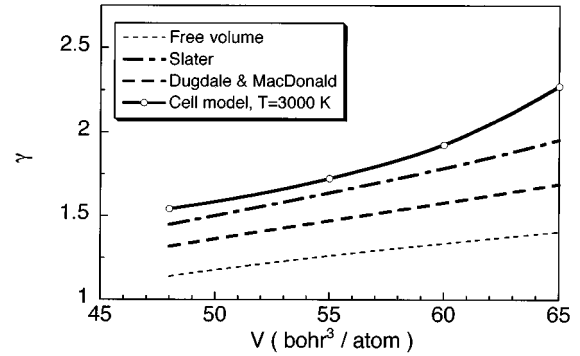


FIG. 11. Grüneisen parameter for fcc iron calculated from approximate expressions and the cell model.

2.5 at $V_0 = 79.73 \text{ bohr}^3/\text{atom}$. However, the value of γ at low compressions is not well constrained from shock compression measurements. This is because at low compressions the thermal pressure on the Hugoniot is small, and a substantial change in γ is not noticeable.

The thermal expansivity $\alpha = 1/V(\partial V / \partial T)_P$ at extreme pressures and temperatures is of interest since it is necessary to transform from static isotherms to high temperature isotherms. Experimental measurements of α at these conditions are difficult and have significant uncertainties.^{39,40} The experimental technique is based on x-ray diffraction measurements of the temperature dependence of volume for a given pressure. We calculate the thermal expansivity from two isotherms at $T + \Delta T$, $T - \Delta T$. A separate third order Birch-Murnaghan equation was fitted to each isotherm, from which $V(T + \Delta T)$ and $V(T - \Delta T)$ at a given pressure were determined. The thermal expansivity is then given by $\alpha = (1/2\Delta T) \ln[V(T + \Delta T)/V(T - \Delta T)]$ at constant pressure. This expression is exact if the temperature dependence of α can be described by $\alpha(T) = \alpha_0 + \alpha_1 T + \alpha_2 T^2$ for the interval $[T - \Delta T, T + \Delta T]$. Numerical tests with $\Delta T = 25, 50$, and 100 K demonstrated convergence of the calculated α with respect to ΔT . The values of α calculated this way are consistent with those from the thermodynamic identity $\alpha = (\partial P / \partial T)_V / K_T$. Being a high order derivative of the Helmholtz free energy, $\alpha(T)$ for the hcp phase was found to be sensitive to the temperature variation of the c/a ratio. We therefore used the equilibrium values of the c/a ratio for each temperature of interest.

The calculated thermal expansivity (Fig. 12) reproduces all known features: it decreases sharply with pressure and increases with temperature. Some care must be taken in comparing with experimental results. The results of Boehler and co-workers^{39,40} are reported not as thermal expansivities, but as values of α averaged over the experimental temperature range (300 K to 2000 K): $\bar{\alpha}(T) = [V(T = 2000 \text{ K})/V(300 \text{ K}) - 1]/(T - 300 \text{ K})$. Because α depends strongly on temperature, $\bar{\alpha}(T)$ is expected to differ significantly from $\alpha(T)$. In order to compare the experimental results to our computations directly, we estimate experimental values of $\alpha(T)$ using finite differences over approximately 200 K temperature intervals from the data of Refs. 39 and 40. Though scattered due to the uncertainty in the measured volumes, these results give a better idea of the actual thermal expansivities than do the averaged expansivities. For

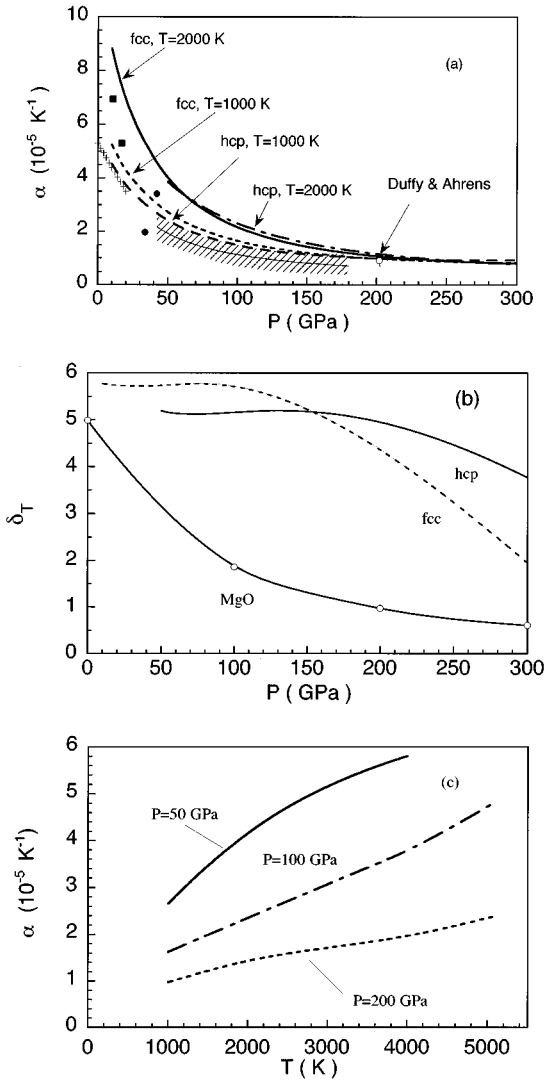


FIG. 12. (a) Calculated thermal expansivity for fcc and hcp phases of iron (lines) compared to experimental measurements. Thermal expansion α of hcp at $T=715$ K from Ref. 41 (pluses). Shock compression estimate of $\bar{\alpha}$ of hcp iron at $T=5200 \pm 500$ K from Ref. 42 (open circle). Closed symbols denote the experimental thermal expansivity we estimated using finite differences from the data in Ref. 39 (closed squares), and from Ref. 40 (closed circles). Thermal expansivity on the Hugoniot deduced in Ref. 38 is given as a thin line and shaded confidence band. (b) Calculated pressure dependence of the Anderson-Grüneisen parameter δ_T at $T=2000$ K. (c) calculated thermal expansivity of fcc iron as a function of temperature at pressures 50, 100, and 200 GPa.

the hcp phase, we find good agreement of the calculated α with the measurements at $T=715$ K.⁴¹ However, the calculated thermal expansivity of the fcc phase at $T=2000$ K decreases less sharply with pressure than do the experimental estimates.³⁹

In order to describe the volume dependence of the thermal expansivity, we used the Anderson-Grüneisen parameter $\delta_T = (\partial \ln \alpha / \partial \ln V)_T$. The pressure dependence of this parameter is given in Fig. 12(b). The figure shows that fcc and hcp phases have similar values of δ_T , although the decrease of this parameter with pressure is less pronounced in hcp than in fcc. For both phases of iron the decrease of δ_T with pres-

sure is much slower than that found for MgO from molecular dynamics simulations¹ and lattice dynamics results.² We find that the pressure dependence of our calculated α can be reasonably approximated (to within 5%) by constant values of $\delta_T=5.2$ and 5.0 for fcc and hcp phases, respectively. An experimental estimate, $\delta_T = 6.5 \pm 0.5$ for the fcc phase was obtained from the pressure dependence of $\bar{\alpha}(T)$ for temperatures ranging from 1000 K to 2000 K.³⁹ For the fcc phase and the same range of pressure (up to 16.8 GPa), we find smaller values: $\delta_T=5.7$ at $T=1000$ K and $\delta_T=5.8$ at $T=2000$ K [Fig. 12(b)]. Some of the discrepancy between calculated and experimental values of δ_T can be attributed to the fact that the experimental estimate is based on $\bar{\alpha}$, rather than α . Over the experimental pressure range, experimental and computed values of $\alpha(T)$ agree to within 20% for fcc and within 10% for hcp.

Jeanloz³⁸ estimated the thermal expansivity on the Hugoniot from analysis of shock compression data for initially porous and nonporous samples. The comparison to his results is given in Fig. 12(a). Another experimental estimate for the averaged thermal expansivity $\bar{\alpha} = \ln(V_T/V_{300}) / (T-300)$ from shock compression measurements⁴² exists for $P=202$ GPa, $T=5200$ K, and $\bar{\alpha} = (9.1 \pm 2.0) \times 10^{-6} \text{ K}^{-1}$. The calculated α at these (P, T) is $1.31 \times 10^{-5} \text{ K}^{-1}$, and the averaged $\bar{\alpha} = 1.00 \times 10^{-5} \text{ K}^{-1}$. The latter calculation was done using exactly the same procedure as in the experimental work,⁴² and agrees within experimental error bars.

V. SUMMARY AND DISCUSSION

We used a combination of the cell model^{17,18} and a tight-binding total-energy method¹⁴ to calculate the thermodynamic properties of iron at high pressures and temperatures. The electronic thermodynamic properties of the TBTE model, such as electronic entropy, are in excellent agreement with those calculated self-consistently. The cell model becomes sufficiently accurate at high pressures and temperatures. Therefore it is a useful tool to evaluate the thermodynamic properties at high temperatures and pressures. The cell model calculations are extremely computationally affordable as opposed to molecular dynamics or Monte Carlo calculations. We presented a procedure to carry out the three-dimensional integrations that makes use of the point group symmetry of the lattice and reduces the required number of computations by an order of magnitude relative to dense sampling of three-dimensional grids. An expression for the virial in the TBTE method was derived that is appropriate for cell model or molecular dynamics calculations.

This approximate procedure has proved to be successful in reproducing the most reliable experimental data—the Hugoniot. Our calculations suggest that the measurements by Yoo *et al.*⁸ probably overestimate the temperature on the Hugoniot by ~ 1000 K. The αK_T parameter was found to be approximately independent of compression for molar volumes ranging from 48 to 60 bohr³/atom. Its temperature dependence is, however, significant and cannot be ignored. The main reason for this temperature dependence is the electronic contribution to thermal pressure. The vibrational contribution to αK_T decreases slightly with temperature. The electronic contribution to αK_T increases linearly with temperature, as expected for crystalline metals.³²

The Grüneisen parameter for compressions of interest to shock-wave measurements was found to have relatively weak temperature dependence. It increases significantly with volume, and therefore the thermal pressure also increases with volume. The second Grüneisen parameter q increases with volume, and therefore the power law $\gamma = \gamma_0(V/V_0)^q$ can be used only as an empirical fit for a small range of compressions. The thermal expansivity was found to decrease rapidly with pressure. We found that the Anderson-Grüneisen parameter δ_T decreases significantly with compression. However, the volume dependence is much smaller than that of MgO; for iron, the assumption that δ_T is independent of compression is sufficient to describe the volume dependence of α to within a few percent.

The combination of an accurate TBTE model¹⁴ with the cell model approximation has proved successful in describing the thermodynamic properties of iron at high pressure and temperature conditions. We verified the results of our calculations by comparison to the available experimental data and also made some predictions. For instance, we predict a significant decrease of the shear elastic constant of the hcp iron with temperature. Good agreement of the calculated properties with the experimental results suggests that the cell model approximation and the usage of the TBTE model for thermodynamic calculations are justified to a large extent for the (P, T) region of interest in this study. Therefore the TBTE model can be used with a slight modification for molecular dynamics simulations of liquid phases of iron at high temperature.

ACKNOWLEDGMENTS

The authors are grateful to A. Bansil for providing a reference to the method of special directions for 3D integration and greatly appreciate helpful discussions with Igor Mazin, Iris Inbar and Mei-Yin Chou. This work was supported by NSF under Grants No. EAR-9305060 and No. EAR-9304624. Calculations were performed on the Cray C90 at Pittsburgh Supercomputer Center and on the IBM SP2 at Cornell.

APPENDIX: QUADRATURE FORMULA FOR THE SOLID ANGLE INTEGRATION FOR THE HCP LATTICE

The quadrature formula for integration over the solid angle Ω of the integrands with the symmetry of the hcp lattice is given below. The integrands can be expanded in lattice harmonics $H_l, H_0 = 1$,

$$f(\theta, \phi, r) = \sum_{l=0}^{\infty} A_l(r) H_l(\theta, \phi). \quad (\text{A1})$$

Due to orthogonality of the lattice harmonics $(H_l, H_m) = \int_{\Omega} H_l H_m d\Omega = 4\pi \delta_{lm}$,

$$\int_{\Omega} f(\Omega) d\Omega = \int_0^{2\pi} d\phi \int_{-1}^1 f(\theta, \phi) d(\cos\theta) = 4\pi A_0. \quad (\text{A2})$$

Let $\Omega_i = (\phi_i, \theta_i)$ be the directions and w_i be the weights of the n -directional quadrature formula. The quadrature formula for the solid angle integration is given by

$$\int_{\Omega} f(\Omega) d\Omega \approx 4\pi \sum_{i=1}^n w_i f(\Omega_i). \quad (\text{A3})$$

The quadrature formula is constructed by requiring that it integrates exactly as many lattice harmonics as possible for the given order (number of directions) n . The number of lattice harmonics integrated exactly is called the power of the quadrature formula, Q . This requirement yields the system of $Q+1$ equations

$$\sum_{i=1}^n w_i = 1, \quad (\text{A4})$$

$$\sum_{i=1}^n w_i H_l(\Omega_i) = 0 \quad (0 < l \leq Q), \quad (\text{A5})$$

which has to be solved. Equation (A4) follows from the definition (A3) and the requirement that the first lattice harmonic $H_0 = 1$ has to be integrated exactly. The other equation (A5) follows from the fact that the lattice harmonics up to H_Q are to be integrated exactly, and $\int_{\Omega} H_l d\Omega = 4\pi \delta_{l0}$.

The lattice harmonics C_l^m for the hcp lattice are given as follows. Starting from C_0^0 and C_3^3 , any multiple of 2 can be added to the value of l and any multiple of 6 can be added to the value of m , so that $m \leq l$,⁴³

$$C_l^m = \frac{1}{\sqrt{2}} (Y_l^m + Y_l^{-m}), \quad (\text{A6})$$

Y_l^m being normalized spherical harmonics. The first few lattice harmonics for hcp are $C_0^0 = 1, C_2^0, C_3^3, C_4^0, C_5^3, C_6^0, C_6^6, C_7^3, C_8^0, C_8^6, C_9^3, C_9^9, C_{10}^0, C_{10}^6, C_{11}^3, C_{11}^9$.

Since the lattice harmonics for the hcp lattice are proportional to $P_l^m(\cos\theta)\cos(m\phi)$, P_l^m being the associated Legendre polynomial, we construct the product-type quadrature formula⁴⁴ using Gauss-Legendre quadrature for integration over $\cos\theta$ and the formula for trigonometric polynomials to integrate over ϕ . A product-type quadrature formula⁴⁴ has the form

$$\int_a^b \int_c^d f(x, y) dx dy \approx \sum_{i=1}^{n_x} \sum_{j=1}^{n_y} w_{ix} w_{jy} f(x_i, y_j), \quad (\text{A7})$$

where n_x and n_y are the number of nodes of one-dimensional quadrature formulas in x and y , respectively, w_{ix} and w_{jy} are the weights, and x_i and y_j are the nodes.

It is important to note that a lattice harmonic for the hcp lattice is a product of an even function in $\cos\theta$ and an even trigonometric polynomial in $x = 3\phi$. Therefore the n -directional formula with $n = n_{\theta} n_{\phi}$ is constructed from two one-dimensional formulas according to Eq. (A7), one in $\cos\theta$ with n_{θ} nodes and the other one in $x = 3\phi$ with n_{ϕ} nodes. Since the integral of a lattice harmonic over the solid angle is zero unless the harmonic is C_0^0 , the quadrature formula eliminates the harmonic if it integrates the harmonic exactly. The one-dimensional quadrature in $\cos\theta$ eliminates the lattice harmonics $C_2^0, C_4^0, C_6^0, \dots, C_{2k}^0, \dots$. Other lattice harmonics contain $\cos(m\phi)$ and are eliminated by the one-dimensional quadrature for trigonometric polynomials.

1. One-dimensional quadrature formula in $\cos\theta$

The lattice harmonics $C_2^0, C_4^0, C_6^0, \dots, C_{2k}^0, \dots$ are proportional to an even Legendre polynomial $P_{2k}(\cos\theta)$. Therefore the appropriate quadrature formula for integrating in $\cos\theta$ from -1 to 1 is obviously the Gauss-Legendre quadrature. It is well known that it has nodes located symmetrically around zero with equal weights for a pair of nodes located at t and $-t$. Since an even function needs to be integrated, we took n_θ positive nodes with the corresponding weights from the Gauss-Legendre quadrature of order $2n_\theta$. Therefore with a one-dimensional quadrature with n_θ nodes one can eliminate lattice harmonics C_{2k}^0 up to $2k \leq 4n_\theta - 1$.

2. One-dimensional quadrature formula in $x = 3\phi$

The quadrature for trigonometric polynomials in x , $g(x) = 1, \cos x, \sin x, \cos 2x, \sin 2x, \dots$ with m nodes is⁴⁴

$$\int_0^{2\pi} g(x) dx \approx T_m = \frac{1}{m} \sum_{l=0}^{m-1} g\left(\frac{2(l-m)+1}{m} \pi\right). \quad (\text{A8})$$

The power of this formula is $m-1$, i.e., it is exact up to $\cos(m-1)x$ and $\sin(m-1)x$. Since we do not have sines in our polynomial, the quadrature formula transforms into

$$T_n = \frac{1}{n} \sum_{l=0}^{n-1} g\left(\frac{2(l-n)+1}{2n} \pi\right). \quad (\text{A9})$$

The latter formula with n nodes in x is exact for *even* trigonometric polynomials up to degree $2n-1$ and has equal weights $1/n$. Therefore the one-dimensional quadrature in 3ϕ eliminates lattice harmonics C_l^m up to $m \leq 3(2n_\phi - 1)$.

3. Example of the construction of the quadrature formula

As an example, the construction of the four-directional formula for hcp is explained in detail below. It is constructed

using two nodes in $\cos\theta$ and two nodes in ϕ . Let $\cos\theta_1 = R_4^1$ and $\cos\theta_2 = R_4^2$, where R_4^1 and R_4^2 are the roots of the Legendre polynomial P_4 . In the standard 1D Gauss-Legendre four-node formula, these nodes have weights w_1 and w_2 . For each $\cos\theta$ we find two values of ϕ as the solution of the system of two equations

$$\cos 3\phi_1 + \cos 3\phi_2 = 0, \quad (\text{A10})$$

$$\cos 6\phi_1 + \cos 6\phi_2 = 0. \quad (\text{A11})$$

This solution is obviously $3\phi_1 = \pi/4$, $3\phi_2 = 3\pi/4$. Then we construct the quadrature formula as follows:

Direction	θ	ϕ	Weight
1	$\arccos(R_4^1)$	$\pi/12$	$w_1/2$
2	$\arccos(R_4^1)$	$\pi/4$	$w_1/2$
3	$\arccos(R_4^2)$	$\pi/12$	$w_2/2$
4	$\arccos(R_4^2)$	$\pi/4$	$w_2/2$

The lattice harmonics C_2^0, C_4^0 , and C_6^0 do not depend on ϕ and are just Legendre polynomials in $\cos\theta$; therefore Eq. (A5) is satisfied for them. As for the rest of the harmonics, they all contain $\cos(3\phi)$ or $\cos(6\phi)$ as a multiplier. Therefore the four-directional quadrature formula is exact for seven nonconstant lattice harmonics up to C_7^3 . The six-directional formula is constructed using three positive roots of P_6 for $\cos\theta$ and the same two nodes of ϕ and is exact for 15 harmonics up to C_{11}^9 .

The described procedure is general and can be carried on to construct the quadrature formulas of the desired precision.

¹I. Inbar and R. E. Cohen, *Geophys. Res. Lett.* **22**, 1533 (1995).
²A. Agnon and M. S. T. Bukowinski, *Phys. Rev. B* **41**, 7755 (1990).
³O. L. Anderson, K. Masuda, and D. G. Isaak, *Phys. Earth Planet. Inter.* **91**, 3 (1995).
⁴J. M. Brown and R. G. McQueen, *J. Geophys. Res.* **91**, 7485 (1986).
⁵H. K. Mao *et al.*, *J. Geophys. Res.* **95**, 21 737 (1990); A. P. Jephcoat, H. K. Mao, and P. M. Bell, *ibid.* **91**, 4677 (1986).
⁶R. Boehler, *Nature (London)* **363**, 534 (1993).
⁷S. K. Saxena, G. Shen, and P. Lazor, *Science* **260**, 1312 (1993).
⁸C. S. Yoo *et al.*, *Phys. Rev. Lett.* **70**, 3931 (1993).
⁹K. G. Gallagher and T. J. Ahrens, in *Proceedings of the 20th International Symposium on Shock Waves*, Bethlehem, 1995 (in press).
¹⁰M. A. Barton and F. D. Stacey, *Phys. Earth Planet. Inter.* **39**, 167 (1985).
¹¹L. Stixrude, R. E. Cohen, and D. J. Singh, *Phys. Rev. B* **50**, 6442 (1994).
¹²F. Mulagria and E. Boschi, *Phys. Earth Planet. Inter.* **18**, 13 (1979).

¹³M. Ross, D. A. Young, and R. Grover, *J. Geophys. Res.* **95**, 21 713 (1990).
¹⁴R. E. Cohen, M. J. Mehl, and D. A. Papaconstantopoulos, *Phys. Rev. B* **50**, 14 694 (1994).
¹⁵R. E. Cohen, L. Stixrude, and D. A. Papaconstantopoulos, in *High Pressure Science and Technology-1993*, edited by S. C. Schmidt, J. W. Shaner, G. A. Samara, and M. Ross (AIP, New York, 1994).
¹⁶J. O. Hirschfelder, C. F. Curtiss, and R. B. Bird, *Molecular Theory of Gases and Liquids* (John Wiley and Sons, Inc., New York, 1954).
¹⁷A. C. Holt and M. Ross, *Phys. Rev. B* **1**, 2700 (1970); A. C. Holt *et al.*, *Physica* **49**, 61 (1970); F. H. Ree and A. C. Holt, *Phys. Rev. B* **8**, 826 (1973); K. Westera and E. R. Cowley, *Phys. Rev. B* **11**, 4008 (1975).
¹⁸E. R. Cowley *et al.*, *Phys. Rev. B* **42**, 3135 (1990).
¹⁹S. Goedecker and M. Teter, *Phys. Rev. B* **51**, 9455 (1995), and references therein.
²⁰C. S. Wang, B. M. Klein, and H. Krakauer, *Phys. Rev. Lett.* **54**, 1852 (1985).
²¹T. Asada and K. Terakura, *Phys. Rev. B* **46**, 13 599 (1992).

- ²²A. K. Mcmahon and M. Ross, *Phys. Rev. B* **15**, 718 (1977).
- ²³J. C. Slater, *Adv. Quantum Chem.* **6**, 1 (1972).
- ²⁴H. J. Monkhorst and J. D. Pack, *Phys. Rev. B* **13**, 5188 (1976); J. D. Pack and H. J. Monkhorst, *ibid.* **B 16**, 1748 (1977).
- ²⁵N. D. Mermin, *Phys. Rev.* **137**, A1441 (1965).
- ²⁶J. P. Perdew and Y. Wang, *Phys. Rev. B* **33**, 8822 (1986); **40**, 3399(E) (1989); **34**, 7406 (E) (1986).
- ²⁷F. Birch, *J. Geophys. Res.* **57**, 227 (1952).
- ²⁸W. R. Fehlnner, S. B. Nickerson, and S. H. Vosko, *Solid State Commun.* **19**, 83 (1976); W. R. Fehlnner and S. H. Vosko, *Can. J. Phys.* **54**, 2159 (1976); A. Bansil, *Solid State Commun.* **16**, 885 (1975); R. Prasad and A. Bansil, *Phys. Rev. B* **21**, 496 (1980).
- ²⁹O. H. Nielsen and R. M. Martin, *Phys. Rev. B* **32**, 3780 (1985).
- ³⁰M. P. Allen and T. J. Tildesley, *Computer Simulations of Liquids* (Clarendon Press, Oxford, 1987).
- ³¹M. J. Mehl, J.E. Osburn, D. A. Papaconstantopoulos, and B. M. Klein, *Phys. Rev. B* **41**, 10 311 (1990).
- ³²D. C. Wallace, *Thermodynamics of Crystals* (John Wiley and Sons, Inc., New York, 1972).
- ³³V. N. Zharkov and V. A. Kalinin, *Equations of State for Solids at High Pressures and Temperatures* (Consultants Bureau, New York, 1971).
- ³⁴D. M. Sherman and H. J. F. Hansen, *Geophys. Res. Lett.* **22**, 1001 (1995).
- ³⁵N. W. Ashcroft and N. D. Mermin, *Solid State Physics* (Saunders College, Philadelphia, 1976).
- ³⁶D. A. Bonnes and J. M. Brown, *J. Geophys. Res.* **95**, 21 721 (1990).
- ³⁷G. H. Wolf and R. Jeanloz, *Phys. Rev. B* **32**, 7798 (1985).
- ³⁸R. Jeanloz, *J. Geophys. Res.* **84**, 6059 (1979).
- ³⁹R. Boehler, N. von Bargaen, and A. Chopelas, *J. Geophys. Res.* **95**, 21 731 (1990).
- ⁴⁰R. Boehler *et al.*, *J. Appl. Phys.* **65**, 1795 (1989).
- ⁴¹M. H. Manghnani, L. C. Ming, and N. Nakagiri, in *High Pressure Research in Mineral Physics* (TERRAPUB, Tokyo, 1987), pp. 155–163.
- ⁴²T. S. Duffy and T. J. Ahrens, *Geophys. Res. Lett.* **20**, 1103 (1993).
- ⁴³S. L. Altman and C. J. Bradley, *Rev. Mod. Phys.* **37**, 33 (1965).
- ⁴⁴A. R. Krommer and C. W. Uerberhuber, *Numerical Integration on Advanced Computer Systems* (Springer-Verlag, Berlin, 1994); P. J. Davis and P. Rabinowitz, *Methods of Numerical Integration* (Academic Press, Orlando, 1984).
- ⁴⁵E. Huang, W. A. Bassett, and P. Tao, *J. Geophys. Res.* **92**, 8129 (1987).